Density-functional theory and Monte Carlo simulation study on the electric double layer around DNA in mixed-size counterion systems

Ke Wang, Yang-Xin Yu,[a] Guang-Hua Gao,[b] and Guang-Sheng Luo
Department of Chemical Engineering, Tsinghua University, Beijing, 100084, People's Republic of China and State Key Laboratory of Chemical Engineering, Tsinghua University, Beijing 100084, People's Republic of China

(Received 5 July 2005; accepted 18 October 2005; published online 19 December 2005)

A density-functional approach and canonical Monte Carlo simulations are presented for describing the ionic microscopic structure around the DNA molecule immersed in mixed-size counterion solutions. In the density-functional approach, the hard-sphere contribution to the Helmholtz energy functional is obtained from the modified fundamental measure theory [Y.-X. Yu and J. Z. Wu, J. Chem. Phys. **117**, 10156 (2002)], and the electrostatic contribution is evaluated through a quadratic functional Taylor expansion. The new theory is suitable to the systems containing ions of arbitrary sizes and valences. In the established canonical Monte Carlo simulation, an iterative self-consistent method is used to evaluate the long-range energy, and another iterative algorithm is adopted to obtain desired bulk ionic concentrations. The ion distributions from the density-functional theory (DFT) are in good agreement with those from the corresponding Monte Carlo (MC) simulations. It is found that the ratio of the bulk concentrations of two species of counterions (cations) makes significant contribution to the ion distributions in the vicinity of DNA. Comparisons with the electrostatic potential profiles from the MC simulations show that the accuracy of the DFT becomes low when a small divalent cation exists. Both the DFT and MC simulation results illustrate that the electrostatic potential at the surface of DNA increases as the anion diameter or the total cation concentration is increased and decreases as the diameter of one cation species is increased. The calculation of electrostatic potential using real ion diameters shows that the accuracy of DFT predictions for divalent ions is also acceptable. [DOI: 10.1063/1.2137710]

I. INTRODUCTION

In the living cell, the phosphate groups on the surface of a DNA molecule dissociate and bear negative charges. These negatively charged phosphate groups attract cations and repulse anions via electrostatic force. In addition, the DNA molecule is impenetrable to small ions, and the short-range repulsion keeps the mobile ions outside the DNA surface. The ions also interact with each other by electrostatic force and excluded-volume interaction. All the forces acting on mobile ions lead to ordered ion distributions and electrostatic potential profiles around DNA. The interaction between ions and DNA inversely reacts on the DNA and changes its three-dimentional structure. Many experiments have proven that the conformation transition of DNA is strongly dependent on the electrolyte environment.[1–3] For example, multivalent cations, especially for divalent cations, interact much more strongly with DNA than monovalent cations do, and this interaction is crucial to the stability of DNA conformation.[4] Besides the effect of small ions on the structure of DNA, the nonspecific binding of small ions to DNA usually competes with the specific binding of other functional macromolecules and dramatically lowers the observed equilibrium constant of these functional molecules binding to DNA.[5–7]

The experimental studies of the DNA electrolyte solution trace back to the classical dialysis equilibrium method.[8,9] This method and the similar membrane equilibrium experiments can only be used to obtain the thermodynamic properties such as membrane equilibrium parameter and osmotic pressure, and leaves no knowledge of the microscopic structure of mobile ions. The nuclear magnetic resonance (NMR) has also been used to analyze the competitive binding of different species of cations.[10,11] However, it is difficult to interpret the binding in terms of microscopic structure without any assumption. Recently applications of new experimental methods such as x-ray diffraction[12] and small-angle neutron scattering[13] make it possible to observe the microscopic structure of mobile ions in the close vicinity of DNA.

To understand the microscopic structure of electric double layer (EDL) around the DNA molecule, various simulation methods have been developed in the past two decades. These studies include the technologies of canonical Monte Carlo (CMC) simulation,[4,14–17] grand canonical Monte Carlo (GCMC) simulation,[18–20] and molecular-dynamic (MD) simulation.[21] Various levels of physical models have been applied including the charged cylinder model,[14,15,18] helical polyion model,[19,20] groove model[16] and all-atom model[4] of

[a]Author to whom correspondence should be addressed. Electronic mail: yangxyu@mail.tsinghua.edu.cn
[b]Electronic mail: gaogh@mail.tsinghua.edu.cn

DNA, and primitive model (PM) and nonprimitive models of electrolyte solution. It should be noted that the PM is unsuitable for evaluations of hard-core effect since the solvent particles, which will naturally dominate the excluded-volume properties of the system, are treated as a continuum. Tang *et al.*[22] have shown that a solvent primitive model leads to strongly oscillatory ion density profiles, in accordance with surface force measurements at short separations. More elaborate treatments with dipolar solvents produce similar results.[23] Even stronger solvent effects can be expected if the solvent has a size different from those of the ions. If, for example, some ions are considerably larger than the solvent particles, then the solvent will push these ions toward the surface, in order to minimize the excluded volume. However, simulations using a molecular model of the solvent are much difficult. For example, it is difficult to study anything but high concentrations because the number of water molecules in a simulation becomes prohibitive at low concentrations.[24] Furthermore, the ion density profiles in molecular solvent are well reproduced by the PM, beyond a few molecular diameters in the low-concentration (weak screening) region.[23] Although the complicated models give some accurate descriptions of the structure of DNA,[25,26] the simple charged cylinder model combined with the primitive model of electrolyte solution can catch some basic characteristic properties of the EDL around DNA and is capable of comparing with experiments at low density. Consequently, these models are adopted in the present work. It should be mentioned that we are interested in the structure in the immediate vicinity of the DNA chain, i.e., in the regime where the primitive model is insufficient for some properties. Further study using nonprimitive model is highly recommended.

Besides the experimental studies and computer simulations, many theoretical approaches have been developed to implement inexpensive and time-saving studies in this field. The well-known Manning's[27,28] theory, which is based on the experimental phenomenon of counterion condensation (CC), provides a convenient predictive framework of ion distributions. In spite of its drawbacks of the oversimplification of physical models and confinement to cylindrical geometry, the CC theory has good consistency with some experimental results[3] and has recently been extended to elaborate the model of DNA.[29] Another classical theory known as the Poisson-Boltzmann (PB) equation[30,31] is also widely used in this field. The PB equation can be solved either analytically for simple geometries or numerically for more complicated physical models such as the all-atom model of DNA,[32] etc. The classical PB theory neglects the excluded-volume effect of small ions. This approximation is adequate for the dilute solution of monovalent cations but leads to bad results for the systems at high bulk concentration or involving multivalent cation.[33–35] Whereas, many recent investigations modified the PB equation by including the effect of the finite size of small ions.[36–38]

Integral equation theory (IET) is another rigorous statistical-mechanical theory for inhomogeneous fluid. It proves that the hypernetted-chain/mean spherical approximation (HNC/MSA) of IET is more accurate than other closures for the ion distributions in EDL.[39] Incorporating the effect of the finite size of ions, the HNC/MSA has better performance in the electrolyte solution of high bulk concentration or multivalent cation presented than PB theory has.[40] HNC/MSA has been extensively used in the calculation of ionic profiles and electrostatic potentials for the systems involving various geometries.[39,41–44]

Unlike all the theories mentioned above, the density-functional theory (DFT) is established based on the thermodynamic principle that the grand canonical potential has a minimum value when the system reaches its equilibrium.[45] In the density-functional study of EDL, the excess Helmholtz energy functional is usually divided into three parts corresponding to the hard-sphere (HS) contribution, Coulombic contribution, and electrical interaction term, respectively. The Coulombic contribution is usually calculated using the integral form of Coulombic theory. The various formulas for evaluating the HS contribution have been established and improved during the past several decades. Recently, a modified fundamental measure theory (MFMT) proposed by Yu *et al.*[40,46] in the framework of Rosenfeld's fundamental measure theory[47–49] (FMT) has been proven to be more accurate than other approximations. The electrical interaction term is usually obtained using a quadratic Taylor expansion with respect to a uniform fluid.[40,50] Whereas, it should be pointed out that the quadratic Taylor expansion with respect to a uniform fluid is not the unique way to evaluate the electrical interaction term. Gillespie *et al.*[51,52] developed another approach where the reference fluid is not the corresponding bulk solution but an inhomogeneous fluid [reference functional density (RFD)]. The DFT using the RFD gives excellent results for the behavior of the EDL with ions of different sizes and valences.[53,54] Many studies of DFT have been carried out for the restrictive primitive model (RPM) electrolyte solution next to the charged or uncharged surface with simple geometries such as planar,[53,55,56] spherical,[40] and cylindrical surfaces.[50,57] Although both HNC/MSA and DFT take into account the excluded-volume effect of small ions, DFT predicts better results with respect to computer simulations than HNC/MSA does.[40,58]

The electrolyte composition of the solution environment *in vivo* that DNA is immersed in is usually complex. Even for the most simplified case, more than one species of cations should be involved. Recently, Nishio and Minakata[59] studied the ion distributions around the rodlike polyelectrolyte of a salt-free system with mixed-size counterions using both the PB equation and MC simulation. Valisko *et al.*[24] predict the effect of asymmetries in ionic diameters and valences on electrical double layer near a charge electrode. Both works treat the systems containing only two species of ions. Different from the previous works, the present work involves the systems containing two species of cations and a species of anion and focuses on the effect of ionic size on ion distribution and electrostatic potential profile around DNA.

The formalism adopted in the present DFT study is similar to our previous one. The HS contribution to the total excess free-energy functional is evaluated using the MFMT and the electrical interaction term is obtained using a quadratic Taylor expansion with respect to a uniform fluid. It should be noted that the direct correlation function we em-

ployed for the asymmetric electrolyte solution has more complex formulas than that we used for RPM in our previous work.[58] The established DFT is used to calculate the ionic density profiles and electrostatic potential profiles. These results are compared with those from the PB equation and the MC simulation.

Different from the work of Patra and Yethiraj[50] which is limited to the electrolyte solution with ions of equal diameters, the present DFT can be applied to the system with ions of arbitrary size and valence. The rest of this paper is organized as follows. In Sec. II we describe the molecular models of systems of interest, details of MC simulation, and DFT method. Numerical results for the ionic density profiles, electrostatic potential profiles, and effect of ionic diameter on the electrostatic potential at the surface of DNA, $\psi(R)$, are presented in Sec. III. Some conclusions and perspectives for the future work are given in Sec. IV.

II. MODEL AND THEORY

A. Molecular model

An isolated model DNA molecule immersed in an electrolyte solution composed of two species of cations and one species of anion is the concern of this paper. The DNA molecule is modeled as an infinitely long, impenetrable charged cylinder. The radius of the hard cylindrical core of the DNA is $R=0.8$ nm. We assume that there is a uniform charge distribution on the surface of DNA with a magnitude $e/2\pi Rb$, where e denotes the charge of electron and b=0.17 nm. The R and b determined above correspond to the B form of DNA. All species of ions are modeled as charged hard spheres with various diameters σ_α, and the minimal separation between ions and the axis of the DNA is $R+\sigma_\alpha/2$. Since DNA is negatively charged, the counterion is cation and the coion is anion. The solvent water is modeled as a continuous structureless media with invariant dielectric constant $\varepsilon=78.4$ at any position, corresponding to that of pure water at $T=298$ K. All the radii and diameters involved in this paper have included the hydration shell. The temperature of the system is $T=298$ K. The ion-polyion interaction potential is given by

$$V_i=\begin{cases}-\dfrac{2e^2z_i}{\varepsilon b}\ln r_i, & r_i \geqslant R+\dfrac{\sigma_i}{2}\\ \infty, \quad \text{otherwise},\end{cases} \tag{1}$$

where e denotes the charge of electron, z_i and σ_i stand for the valance and diameter of ion i, respectively, and r_i denotes the distance between the axis of DNA and the center of ion i.

The ion-ion interaction potential is given by

$$u_{ij}=\begin{cases}\dfrac{e^2z_iz_j}{\varepsilon|\mathbf{r}_i-\mathbf{r}_j|}, & |\mathbf{r}_i-\mathbf{r}_j| \geqslant \dfrac{\sigma_i+\sigma_j}{2}\\ \infty, \quad \text{otherwise},\end{cases} \tag{2}$$

where $\boldsymbol{r}_i$ is the position of ion i.

B. Density-functional theory

The grand potential functional Ω for the system described above can be expressed as a functional of the density profiles of each species, through the Legendre transform,

$$\Omega[\{\rho_i\}]=F[\{\rho_i\}]+\sum_{i=1}^{N}\int d\mathbf{r}[V_i(\mathbf{r})-\mu_i]\rho_i(\mathbf{r}), \tag{3}$$

where N is the number of ion species, μ_i is the chemical potential of ion i, $F[\{\rho_i\}]$ represents the Helmholtz energy functional, and $\{\rho_i\}$ represents a set of ion density profiles.

By virtue of variational principle, the equilibrium density distribution of each ionic component $\{\tilde{\rho}_i\}$ corresponding to the minimum of the grand potential $\tilde{\Omega}$ is obtained from the Euler equation,

$$\left.\frac{\delta\Omega[\{\rho_i\}]}{\delta\rho_i(r)}\right|_{\tilde{\rho}}=0, \quad \Omega[\{\rho_i\}]_{\tilde{\rho}}=\tilde{\Omega}. \tag{4}$$

The Helmholtz energy functional can be divided into two parts corresponding to the ideal-gas contribution, $F^{\mathrm{id}}[\{\rho_i\}]$, and excess Helmholtz energy, $F^{\mathrm{ex}}[\{\rho_i\}]$, respectively,

$$F[\{\rho_i\}]=F^{\mathrm{id}}[\{\rho_i\}]+F^{\mathrm{ex}}[\{\rho_i\}]. \tag{5}$$

$F^{\mathrm{id}}[\{\rho_i\}]$ is obtained accurately from classical statistical mechanics,

$$F^{\mathrm{id}}[\{\rho_i\}]=k_BT\sum_{i=1}^{N}\int d\mathbf{r}\rho_i(\mathbf{r})[\ln(\rho_i(\mathbf{r})\Lambda_i^3)-1], \tag{6}$$

where Λ_i is the thermal wavelength of component i and k_B is the Boltzmann constant. $F^{\mathrm{ex}}[\{\rho_i\}]$ can be further decomposed into three parts according to different types of interactions,

$$F^{\mathrm{ex}}[\{\rho_i\}]=F_C^{\mathrm{ex}}[\{\rho_i\}]+F_{\mathrm{hs}}^{\mathrm{ex}}[\{\rho_i\}]+F_{\mathrm{el}}^{\mathrm{ex}}[\{\rho_i\}]. \tag{7}$$

The first term on the right hand of Eq. (7) is the Coulombic contribution, the second one is the hard-sphere contribution, and the last one is the electrostatic contribution of the coupling of the former two kinds of contributions.

The Coulombic contribution is expressed as

$$F_C^{\mathrm{ex}}[\{\rho_i\}]=\frac{1}{2}\int\int d\mathbf{r}d\mathbf{r}'\sum_{i,j}\frac{z_iz_je^2\rho_i(\mathbf{r})\rho_j(\mathbf{r}')}{\varepsilon|\mathbf{r}-\mathbf{r}'|}. \tag{8}$$

It has been proven that the MFMT (Ref. 46) is better than other DFTs for the estimation of hard-core repulsion. The MFMT gives a more accurate contact value of density profile than the FMT. Therefore, the hard-sphere contribution from the MFMT (Ref. 46) is adopted in this work,

$$F_{\mathrm{hs}}^{\mathrm{ex}}=k_BT\int\Phi^{\mathrm{hs}}[n_\alpha(\mathbf{r})]d\mathbf{r}, \tag{9}$$

where $\Phi^{\mathrm{hs}}[n_\alpha(\mathbf{r})]$, described as a function of the weighted density $n_\alpha(\mathbf{r})$, is the reduced excess Helmholtz free-energy density due to hard-sphere contribution from the MFMT. The exact expressions of $\Phi^{\mathrm{hs}}[n_\alpha(\mathbf{r})]$ and $n_\alpha(\mathbf{r})$ have been described in the previous paper.[40,46]

$F_{\mathrm{el}}^{\mathrm{ex}}[\{\rho_i\}]$ is obtained through a second-order functional Taylor expansion of the residual Helmholtz free energy around a uniform fluid,[40]

$$\beta F_{\mathrm{el}}^{\mathrm{ex}}[\{\rho_i\}] = \beta F_{\mathrm{el}}^{\mathrm{ex}}[\{\rho_i^b\}] - \sum_{i=1}^{N} \Delta C_i^{(1)\mathrm{el}} \int d\mathbf{r}(\rho_i(\mathbf{r}) - \rho_i^b) - \frac{1}{2}\sum_{i=1}^{N}\sum_{j=1}^{N} \int\int d\mathbf{r}d\mathbf{r}' \Delta C_{ij}^{(2)\mathrm{el}}(|\mathbf{r}' - \mathbf{r}|) \times (\rho_i(\mathbf{r}) - \rho_i^b)(\rho_j(\mathbf{r}') - \rho_j^b), \quad (10)$$

where $\{\rho_i^b\}$ is the bulk density of i, $\Delta C_i^{(1)\mathrm{el}}$ and $C_{ij}^{(2)\mathrm{el}}$ are direct correlation functions due to the residual electrostatic interaction. $\Delta C_i^{(1)\mathrm{el}}$ will disappear in the Euler equation, and $\Delta C_{ij}^{(2)\mathrm{el}}(r)$ can be evaluated explicitly by the mean spherical approximation (MSA). The details of $\Delta C_{ij}^{(2)\mathrm{el}}(r)$ are described elsewhere.[60]

There exist several methods to introduce effects of ion-ion correlations into the Poisson-Boltzmann theory. For example, Forsman approximated the correlations by an effective interaction potential, which differs from the Coulombic at short range.[61] Penfold *et al.*[62] included the correlations with exclusion holes (given by the "hard-sphere" diameters) within which the interactions are zero, which results in a "hole-corrected" Poisson-Boltzmann theory. But in our DFT, the volume exclusion is represented by the MFMT and the ion-ion correlations are estimated by the direct correlation function from the mean spherical approximation. Because we have considered correlations both between like-charged ions and between unlike-charged ions, the present DFT is able to reproduce the interesting effects, such as the charge inversion and the attraction between like-charged surfaces[63] (see our previous work[58]).

Incorporating the explicit expressions of the Helmholtz energy mentioned above, the Euler equations Eq. (4) becomes

$$\rho_i(\mathbf{r}) = \rho_i^b \exp\left\{ \frac{1}{k_B T}\left[-\frac{\delta F_{\mathrm{hs}}^{\mathrm{ex}}}{\delta \rho_i(\mathbf{r})} + \mu_{i,\mathrm{hs}}^{\mathrm{ex}} \right] - \frac{z_i e}{k_B T}[\psi(\mathbf{r}) - \psi^b] + \sum_{j=1}^{N} \int d\mathbf{r}' \Delta C_{ij}^{(2)\mathrm{el}}(|\mathbf{r}' - \mathbf{r}|)(\rho_j(\mathbf{r}') - \rho_j^b) \right\}, \quad (11)$$

where $F_{\mathrm{hs}}^{\mathrm{ex}}$ is evaluated from Eq. (9), $\mu_{i,\mathrm{hs}}^{\mathrm{ex}}$ is excess chemical potential due to hard-sphere contribution, $\psi(\mathbf{r})$ is the mean electrostatic potential obtained from the solution of the Poisson equation in cylindrical geometry,

$$\psi(r) = -\frac{4\pi e}{\varepsilon} \int_r^{\infty} \ln\left(\frac{r'}{r}\right) \sum_i \rho_i(r') z_i r' dr', \quad (12)$$

with the electroneutrality condition given by

$$2\pi b \int_R^{\infty} dr r \sum_i \rho_i(r) z_i = 1, \quad (13)$$

where r and r' are the distances between the ion center and polyion axis, and the subscript i denotes species i.

C. Canonical Monte Carlo simulation

To test the density-functional theory established above, Monte Carlo simulations are performed in canonical ensemble. In these canonical Monte Carlo (CMC) simulations, we use a cylindrical simulation cell with its axis coinciding with the axis of the DNA molecule. The radius and height of the simulation cell are R_{cell} and H_{cell}, respectively. A hard-wall outer boundary is imposed on the simulation cell in radial direction, while a periodic boundary condition is applied in axial direction by imagining that the simulation cell is replicated infinitely along the axial direction on both sides of the central cell. In the calculation of the total energy of the system, if any ion overlaps with the DNA molecule, radial outer boundary, or other ions, the total energy of this configuration is positive infinite. Otherwise, the total energy of the system is calculated by

$$U_{\mathrm{Total}} = -\sum_{i=1}^{N} \frac{2e^2 z_i}{\varepsilon b} \ln r_i + \sum_{i=1}^{N}\sum_{j>i}^{N} \frac{e^2 z_i z_j}{\varepsilon |\mathbf{r}_i - \mathbf{r}_j|_{\mathrm{MI}}} + \sum_{i=1}^{N} e z_i \Phi_{\mathrm{ext}}(\mathbf{r}_i). \quad (14)$$

The first term of the right hand of Eq. (14) corresponds to the polyion-ion interaction, the second term is the total electrostatic interaction between ions in the central cell calculated using minimum image (MI) criterion,[64] and $\Phi_{\mathrm{ext}}(\mathbf{r}_i)$ in the last term is the external potential produced by the mobile ions out of the central cell.[14]

The simulation starts by randomly placing the mobile ions within the simulation box but avoiding overlap. In each MC step, a randomly selected ion is moved according to standard Metropolis algorithm.[64] The external potential $\Phi_{\mathrm{ext}}(\mathbf{r}_i)$ is obtained from the ion distributions of the central cell using self-consistent algorithm[14,65] and renewed for appropriate interval. The long-range correction of electrostatic energy used in this work is the same as the algorithm established by Murthy *et al.*[65] and may produce a sampling process which is not a strict Markov chain. However, in the present work, the height of the simulation cell is assigned large enough that the bias in sampling has neglected effect on the results. Recently, many modified methods have been proposed based on Murthy's algorithm, which can be found elsewhere.[66–69]

After approximate 7.0×10^7 pre-equilibrium MC steps, the equilibrium of the system is achieved. Then five consecutive blocks, each having 5.0×10^7 steps, are performed to obtain the ionic profiles and electrostatic potentials and their statistical uncertainties.[15] To calculate the reduced ion density profiles and electrostatic potentials, the simulation box is divided into a set of concentric annular shells with a thickness of 0.01 nm.

In the beginning of CMC simulations one does not know the bulk concentration of each ionic species. But, using a large enough R_{cell}, the bulk concentrations of ions can be obtained in the middle of the simulation cell between the surface of DNA and the radial outer boundary of the simulation box when equilibrium is achieved. It should be noted that in each simulation performed in the present work, several pre-equilibrium trials are attempted, changing the ion numbers and moving the outer boundary successively, to obtain the desired bulk ionic concentrations. The difference be-

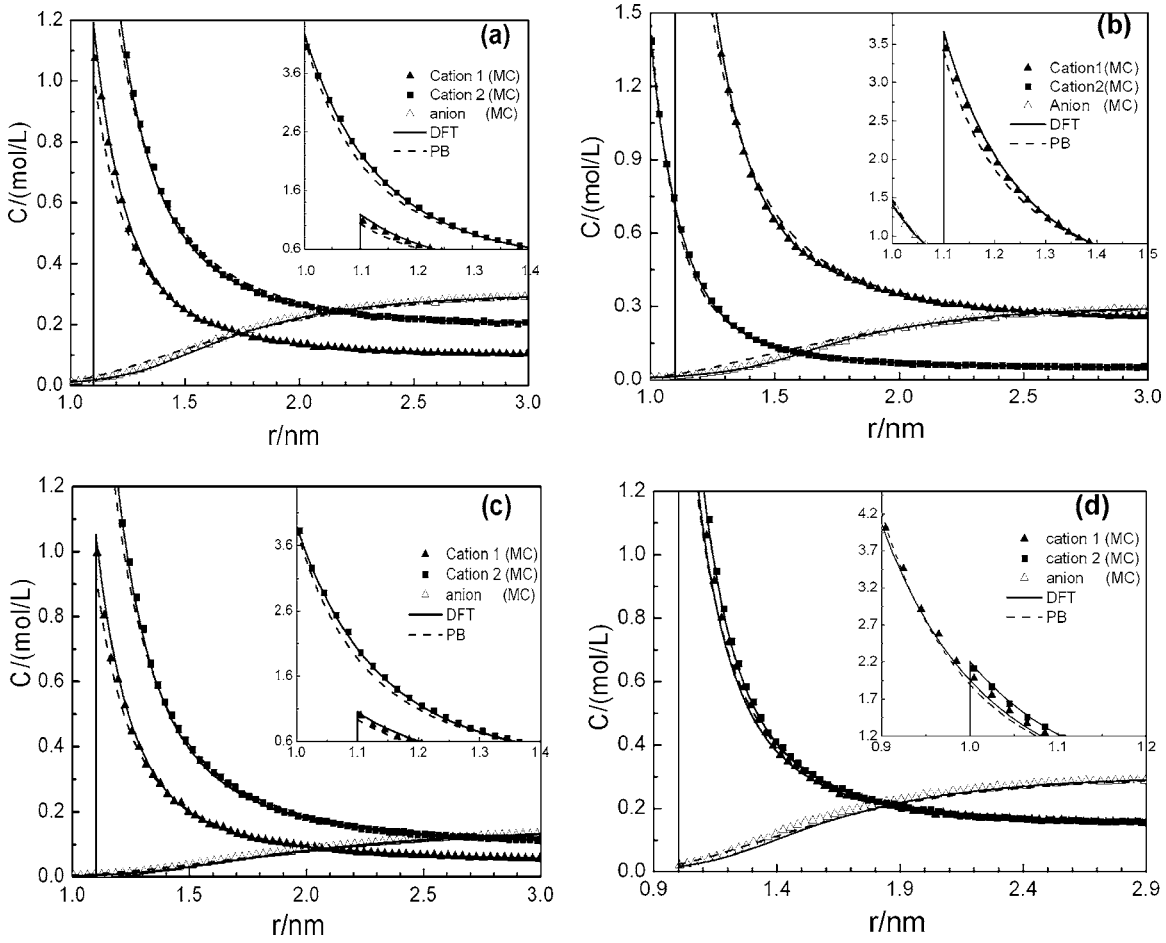

FIG. 1. Ion distributions around the model DNA molecule predicted by the MC simulation, DFT, and PB equation. The electrolyte solutions contain two monovalent cations (cation 1 and cation 2) and one monovalent anion. The diameters of both cation 2 and anion are fixed at 0.4 nm, while the bulk ionic concentrations and the diameter of cation 1 are varied. The diameter of cation 1 and the bulk concentrations of cations are (a) σ_{c1}=0.6 nm, C^b_{c1} =0.100 mol/L, and C^b_{c2}=0.200 mol/L, (b) σ_{c1}=0.6 nm, C^b_{c1}=0.250 mol/L, and C^b_{c2}=0.050 mol/L, (c) σ_{c1}=0.6 nm, C^b_{c1}=0.050 mol/L, and C^b_{c2} =0.100 mol/L, and (d) σ_{c1}=0.2 nm, C^b_{c1}=0.150 mol/L, and C^b_{c2}=0.150 mol/L.

tween bulk ionic concentrations from simulation and the desired concentrations has been proven to be negligible (relative error of $<0.5\%$).

III. RESULTS AND DISCUSSION

The main purpose of this research is to give a molecular understanding of the effect of ion size on the microscopic structure and electrostatic potential around the DNA molecule in mixed counterion systems. The electrolyte solutions involved in this work consist of two species of cations with the same valence but different diameters and one species of anion. However, the application of the present DFT is not limited to the systems described here.

A. Microscopic structure

Figure 1 shows the ion distributions around the model DNA molecule predicted by the MC simulation, DFT, and PB equation for the systems of monovalent counterions at different cationic diameters and concentrations. In the captions of Figs. 1 and 2, σ_{c1}, C^b_{c1}, and C^b_{c2} stand for the diameter of cation 1 and the bulk concentrations of cation 1 and cation 2, respectively. From Figs. 1(a)–1(d) one can find that the ion profiles predicted by the DFT coincide excellently with those from the MC simulation. The predictions from the PB equation are also good, but not as accurate as those from the DFT. From Fig. 1, we find that the shapes of the density profiles of the counterions are similar, but the contact values are related to the ratio of bulk concentrations of counterions

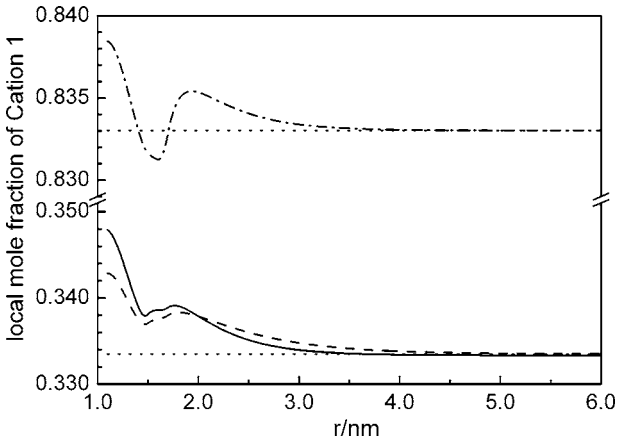

FIG. 2. Local mole fraction of cation 1 surrounding DNA. Solid line, dot-dashed line, and dashed line represent the DFT results corresponding to the situations of Fig. 1(a)–1(c), respectively. The dotted line represents the results from the PB equation.

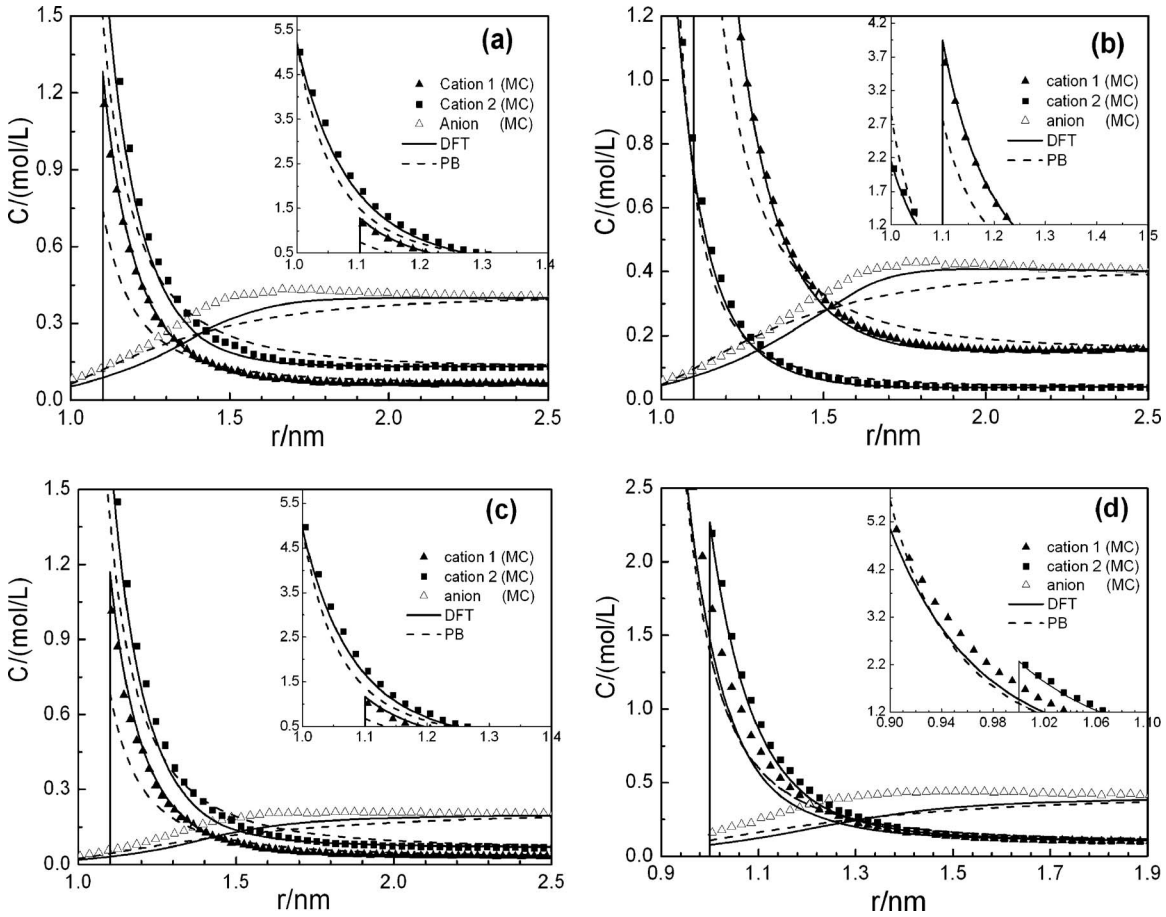

FIG. 3. Ion distributions around the model DNA molecule predicted by the MC simulation, DFT, and PB equation. The electrolyte solutions contain two divalent cations (cation 1 and cation 2) and one monovalent anion. The diameters of both cation 2 and anion are fixed at 0.4 nm, while the bulk ionic concentrations and the diameter of cation 1 are varied. The diameter of cation 1 and the bulk concentrations of cations are (a) $\sigma_{c1}=0.6$ nm, $C^b_{c1}=0.067$ mol/L, and $C^b_{c2}=0.133$ mol/L, (b) $\sigma_{c1}=0.6$ nm, $C^b_{c1}=0.160$ mol/L, and $C^b_{c2}=0.040$ mol/L, (c) $\sigma_{c1}=0.6$ nm, $C^b_{c1}=0.033$ mol/L, and $C^b_{c2}=0.067$ mol/L, and (d) $\sigma_{c1}=0.2$ nm and $C^b_{c1}=C^b_{c2}=0.100$ mol/L.

as well as the total counterion concentration. When the total bulk concentration of the counterions keeps constant, the contact values of density profiles are dramatically affected by the ratio of bulk concentration of counterions, as can be seen from a comparison between the insets of Figs. 1(a) and 1(b). The little difference between Figs. 1(a) and 1(c) shows that the change of the total bulk concentration of counterions has relatively little effect on the ion density profiles in the close vicinity of the DNA surface when the ratio of bulk concentrations of two counterions keeps invariant. To illustrate this conclusion furthermore, the profiles of the mole fraction of cation 1 in total cation concentration are plotted in Fig. 2. We find that the fraction profiles corresponding to Figs. 1(a) and 1(c) are similar, while the profile corresponding to Fig. 1(b) is much higher. The structure of ion profiles in the vicinity of DNA mainly depends on the ratio of the bulk concentration of the two cations. For the reason of volume-excluded effect, the fractions of cation 1 in the close vicinity of DNA are much higher than the bulk. The PB theory is unable to predict this phenomenon.

The ion distributions of the system containing mixed counterions of 0.2 and 0.4 nm are given in Fig. 1(d). The different ion sizes result in the different closest distances of ions to DNA. The smaller the ionic diameter, the closer the ion approaches the surface of DNA. As shown in Fig. 1(d), without any competition the smaller counterion is concentrated in the volume extending from $R+\sigma_{C1}/2$ to $R+\sigma_{C2}/2$ in the radial direction.

Figure 3 gives the results of ion distributions around the model DNA molecule predicted by the MC simulation, DFT, and PB equation for the system of divalent counterions. Although the results from the DFT for the system of divalent counterions are not so good as those for the systems of monovalent counterion, the DFT gives a fairly accurate prediction, especially for the cation distribution in the close vicinity of DNA. In all cases shown in Fig. 3, the DFT underestimates the coion density profiles when compared to the results from the MC simulations. When a small diameter is assigned to a divalent counterion, the DFT performs poorly since the second direct correlation from the MSA closure is not accurate in accord with the poor bulk properties resulting from the MSA closure. It is true that the present DFT reduces to the ordinary PB theory in the limit of ionic diameter $\sigma=0$. Therefore the "real" role of the hard cores may exist, namely, approximate "Coulomb holes" (++) and "loss of attraction holes" (+−). Nevertheless, the failure of the DFT in the prediction of the coion density distribution may have negligible effect on the electrostatic potential as well as other

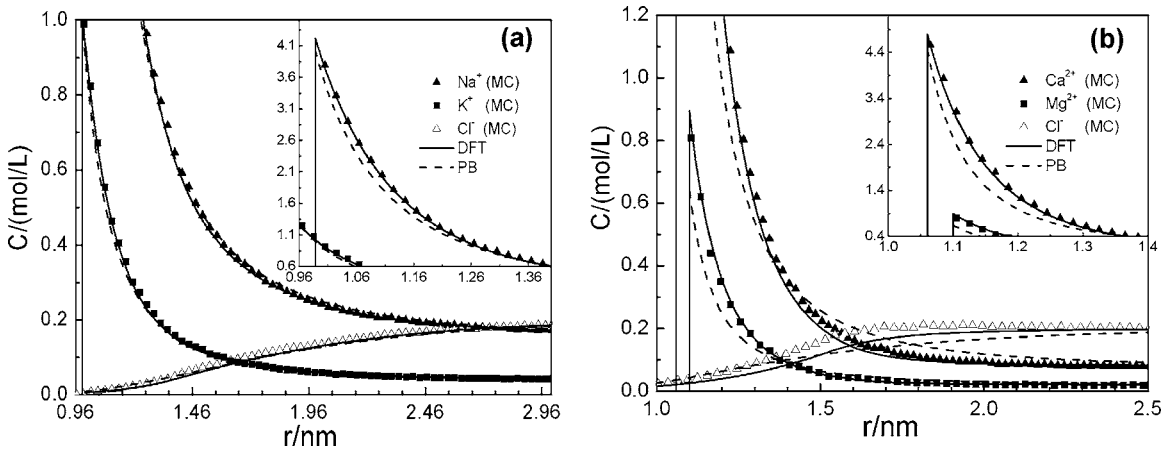

FIG. 4. Ion distributions around the model DNA molecule predicted by the MC simulation, DFT, and PB equation using the parameter of real ions. (a) is the situation of mixed counterions of Na^+ and K^+ with Cl^- as a coion. The diameters of Na^+, K^+, and Cl^- are from Ref. 20 and their concentrations are 0.160, 0.040, and 0.200 mol/L, respectively. (b) is the situation of mixed counterions of Ca^{2+} and Mg^{2+} with Cl^- as a coion. The diameters of Ca^{2+}, Mg^{2+}, and Cl^- are from Ref. 20 and their concentrations are 0.80, 0.020, and 0.200 mol/L, respectively.

thermodynamic properties for the extremely low concentration of coion in the close vicinity of DNA. The inaccuracy of the DFT in the calculation of the distributions of divalent counterions and coion has been discussed in our previous work.[58] The PB theory gives even worse predictions of the density distributions of both cations and anion. From Figs. 3(a)–3(d), it can be concluded that the ratio of bulk cation concentrations, the cation sizes, and the total cation concentration have similar effects on the ionic distribution to the cases of monovalent cations.

It should be pointed out that the only parameter characterized by ionic sizes in the PB theory is the minimal distance from the center of the ion to the surface of DNA. This is because the PB theory is unable to include the information of excluded-volume effect among small ions. Therefore, if the two cations have the same bulk concentrations, the PB theory predicts the same local density for them in the position that both of them can reach. This phenomenon has been presented in Figs. 1(d) and 3(d). However, incorporating the excluded-volume effect, the MC simulation and DFT predict two separate counterion distributions around DNA even though the two counterions have the same bulk concentration.

In Fig. 4, the above calculation are repeated but using the ion diameters of real ions. The system of Na^+, K^+, and Cl^- and the system of Ca^{2+}, Mg^{2+}, and Cl^- are investigated in panels (a) and (b), respectively. A natural consequence of the dielectric continuum approximation is the introduction of "effective" radii of small ions. The effective diameters of Na^+, K^+, Ca^{2+}, Mg^{2+}, and Cl^- used in this work are taken from Korolev *et al.*[20] because they reproduce good experimental data for bulk electrolyte solutions. The ion distributions predicted by DFT using real ion diameters are in good consistency with the MC result in both situations of monovalent and divalent cations.

B. Electrostatic potential profiles

The influence of the sizes of cations on electrostatic potential in monovalent cation system is displayed in Fig. 5. The results from the DFT agree quite well with those from MC simulations. The potential profiles predicted by the PB equation have obvious negative deviations from the MC simulation data, though the corresponding ion distributions only unnoticeably deviate from the MC results. Recall that

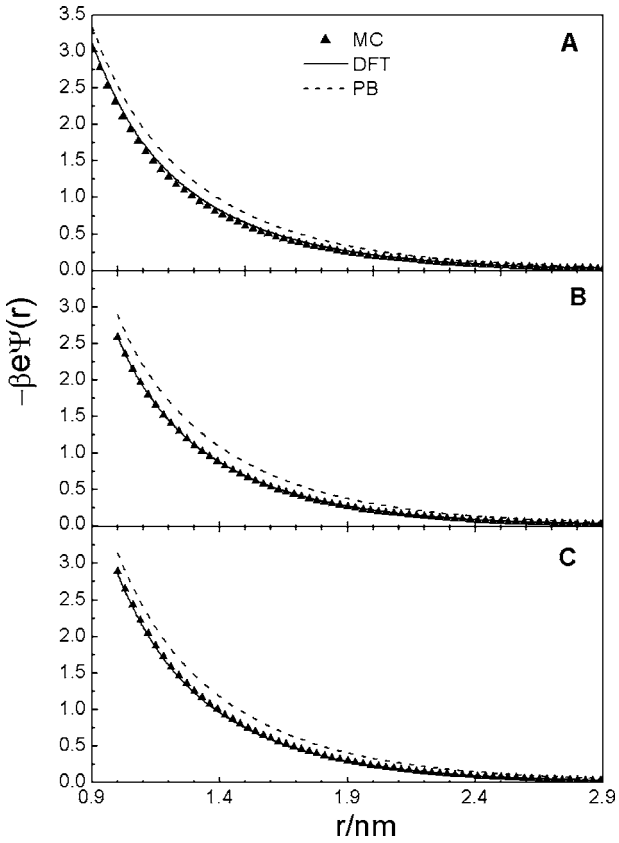

FIG. 5. Reduced mean electrostatic potential around DNA predicted by the MC simulation, DFT, and PB equation. The electrolyte solutions contain two monovalent cations and one monovalent anion. The bulk concentrations of cation 1, cation 2, and anion are fixed at 0.150, 0.150, and 0.300 mol/L, respectively. The diameters of both cation 2 and anion are fixed at 0.4 nm, while the diameters of cation 1 are (a) 0.2 nm, (b) 0.4 nm, and (c) 0.6 nm.

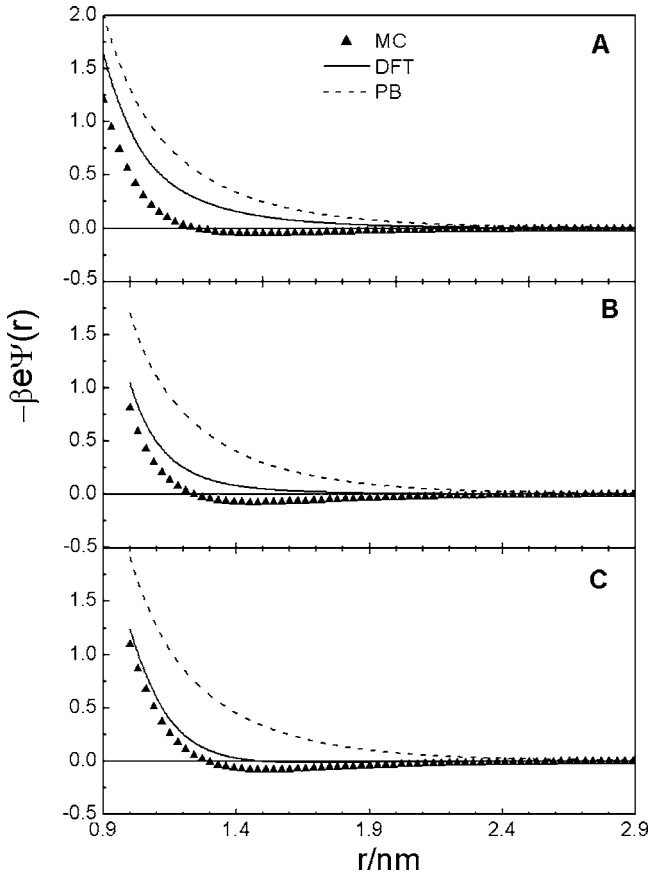

FIG. 6. Reduced mean electrostatic potential around DNA predicted by the MC simulation, DFT, and PB equation. The electrolyte solutions contain two divalent cations and one monovalent anion. The bulk concentrations of cation 1, cation 2, and anion are fixed at 0.100, 0.100, and 0.400 mol/L, respectively. The diameters of cation 2 and anion are fixed at 0.4 nm, while the diameters of cation 1 are (a) 0.2 nm, (b) 0.4 nm, and (c) 0.6 nm.

the electrostatic potential is obtained by integrating the ion density distributions [see Eq. (12)], the tiny deviations in ion density distributions will be accumulated and become noticeable in consequential electrostatic potentials.

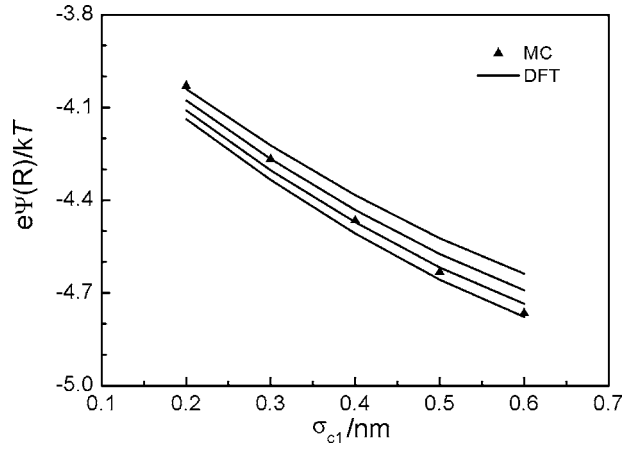

FIG. 7. Dependence of $\psi(R)$ on the diameter of cation for the system containing monovalent cations. The diameter of cation 2 is fixed at 0.4 nm, and cation 1 and cation 2 have the same bulk concentration of 0.100 mol/L. The solid triangle represents the results predicted by the MC simulation for the anion diameter of 0.4 nm. The five curves from bottom to top are the results predicted by the DFT with anion diameters of 0.3, 0.4, 0.5, and 0.6 nm, respectively.

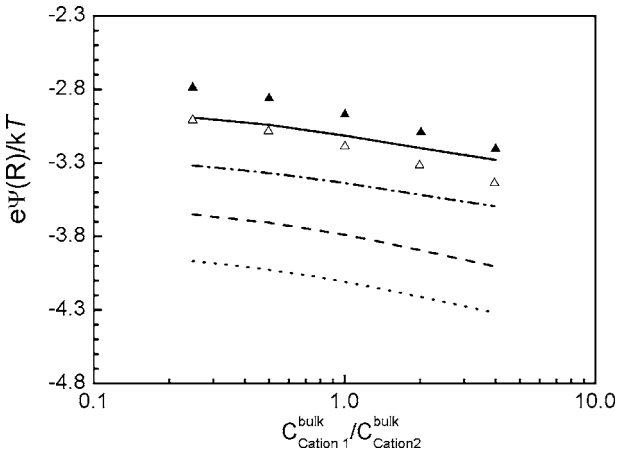

FIG. 8. Dependence of $\psi(R)$ on the bulk concentration ratio of two divalent cations. The diameters of cation 1, cation 2, and anion are 0.6, 0.4, and 0.4 nm, respectively. The solid triangle, solid line, and dashed line represent the results predicted by the MC simulation, DFT, and PB equation, respectively, for the system containing 0.200 mol/L cations. The open triangle, dot-dashed line, and dot line represent the results predicted by the MC simulation, DFT, and PB equation, respectively, for the system containing 0.100 mol/L cations.

The dependence of the cationic size on electrostatic potential in divalent cation system is displayed in Fig. 6. We find from Figs. 6 that as the diameter of one cation becomes larger, the prediction from DFT becomes more accurate. The larger the size of the cation is, the more the contribution from the excluded-volume effects. Therefore above findings suggest that the contribution from the HS part in the present DFT should be accurate, and deviations from the simulations should be produced by the coupling of Coulombic and hard-sphere interactions. This indicates that the second direct correlation function used for asymmetric electrolyte contributes mainly to the total inaccuracy of the present DFT. It is also shown in Fig. 6 that the PB equation is not a good theory for the divalent cation system since it hardly even gives a qualitative prediction of electrostatic potentials.

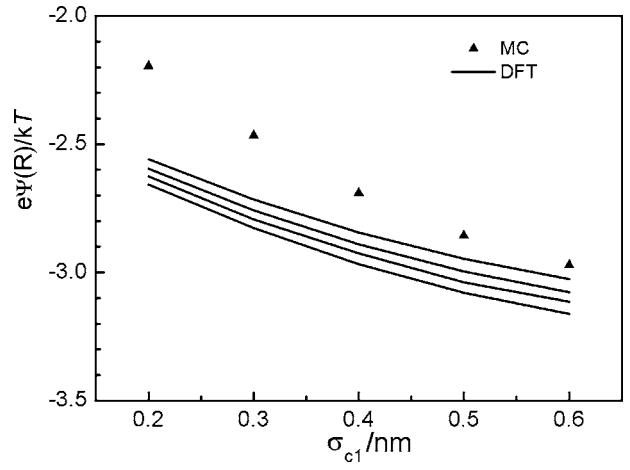

FIG. 9. Dependence of $\psi(R)$ on the diameter of cation for the system containing divalent cations. The diameter of cation 2 is fixed at 0.4 nm, and cation 1 and cation 2 have the same bulk concentration of 0.100 mol/L. The solid triangle represents the results predicted from the MC simulation for the anion diameter of 0.4 nm. The five curves from bottom to top are the results predicted by the DFT with different anion diameters of 0.3, 0.4, and 0.5 nm, respectively.

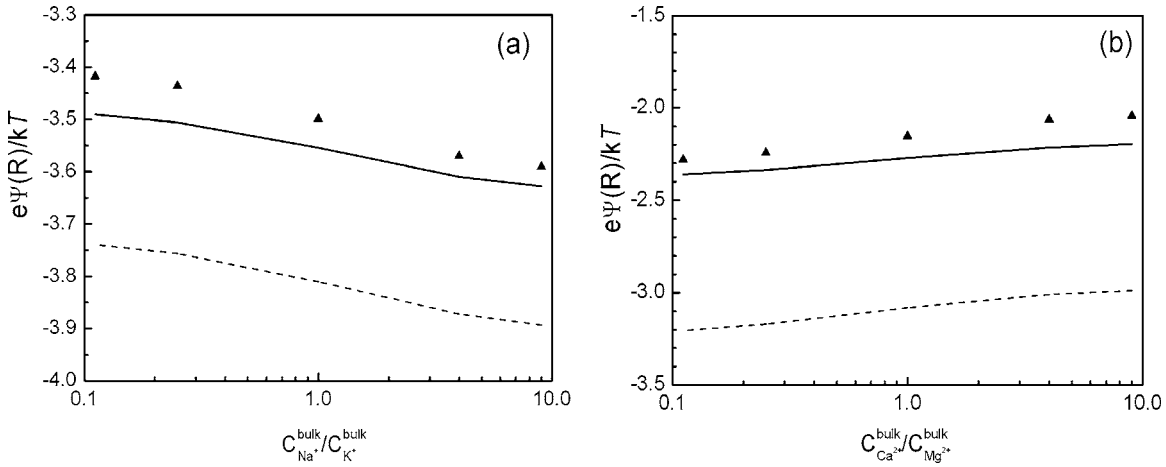

FIG. 10. Dependence of $\psi(R)$ on the bulk concentration ratio of two real cations. (a) is the situation of mixed counterions of Na^+ and K^+ with Cl^- as a coion. The diameters of Na^+, K^+, and Cl^- are from Ref. 20 and the total cation concentration is 0.200 mol/L. (b) is the situation of mixed counterions of Ca^{2+} and Mg^{2+} with Cl^- as a coion. The diameters of Ca^{2+}, Mg^{2+}, and Cl^- are from Ref. 20 and the total cation concentration is 0.100 mol/L.

The electrostatic potential profiles from the MC simulations in Fig. 6 change their sign in the vicinity of DNA and create areas of positive potential. This is the characteristic of "charge inversion" or "overcharging". We have discussed this interesting phenomenon in detail in our previous work.[58] It should be mentioned that the DFT has the capability of predicting this phenomenon for it incorporates the excluded-volume effect of ions. However, in this work, the DFT generally underestimates overcharging and even fails to predict it in Figs. 6(a) and 6(b). This inaccuracy may be attributed to the inaccuracy of the second direct correlation function from MSA in highly asymmetric electrolyte as mentioned above.

C. Electrostatic potential at DNA surface

The negatively charged groups on the DNA surface and the surrounding mobile ions form an electric double layer around DNA. The local electrostatic potential varies along the radial direction from R to infinity as shown in the above section. We now define the potential at R as $\psi(R)$. $\psi(R)$ is a typical value of electrostatic potential which reflects the extent that the surrounding small ions screen the electrostatic field produced by polyion. As a matter of fact, $\psi(R)$ should be negative infinity when small ions are absent in the system.

The influence of ionic sizes on $\psi(R)$ is presented in Fig. 7. The DFT also gives a creditable prediction under all conditions involved in Fig. 7 except for a slightly increasing inaccuracy as the asymmetry of ion sizes enhances. From the single curve in Fig. 7, it is found that $\psi(R)$ decreases monotonically as the diameter of one cation increases. This trend is also explained as follows: the smaller cation can screen the external electrostatic field more effectively than the larger one can. Comparing with the curves plotted at different anionic diameters, we found that the anionic diameter has a contrary effect on $\psi(R)$ compared to that of cationic diameter, namely, the smaller the anionic diameter, the more negative the value of $\psi(R)$.

Figure 8 presents the dependence of $\psi(R)$ on the ratio of the bulk concentrations of two cations. As shown in this figure, $\psi(R)$ becomes more negative as the bulk mole fraction of the small cation decreases or as the total bulk cation concentration decreases. This suggests that the smaller counterion and the more concentrated bulk electrolyte solution have more capacity of screening the external electrostatic potential.

The influences of cationic ion size on $\psi(R)$ in divalent cation systems are plotted in Fig. 9. The ion size has the same effect on $\psi(R)$ as the case of monovalent cations. The accuracy of the DFT in the prediction of $\psi(R)$ for the systems containing divalent cations is obviously not so good as that for the system of monovalent cations. As shown in Figs. 8 and 9 the inaccuracy of the DFT in calculating $\psi(R)$ declines as the proportion of the bigger cation is increased and as the cationic size becomes larger. In all the cases involved, the PB equation substantially underestimates $\psi(R)$.

Figure 10 shows the dependence of $\psi(R)$ on the ratio of the bulk concentrations of two cations using the real ion diameters from Ref. 20. Although the above predictions of DFT for divalent ions are commonly not so good as those of monovalent ions, the diameters of real divalent ions are usually larger than those of monovalent ions. Therefore, the accuracy of the DFT prediction of real divalent ions is acceptable.

IV. CONCLUDING REMARKS

A density-functional approach is proposed to investigate the microscopic structure of ions in the vicinity of DNA. In the density-functional approach, a modified fundamental measure theory proposed by Yu *et al.*[40,46] is used to evaluate the HS contribution to the free-energy functional, and the electrical interaction is obtained through a quadratic Taylor expansion around a corresponding uniform fluid, where the direct correlation function for asymmetric electrolytes is calculated using an explicit expression from MSA. To test the accuracy of the DFT and other theoretical methods, a canonical Monte Carlo simulation is carried out using the same molecular model as that in the DFT. In MC simulations, an iterative self-consistent method[14,65] is proposed to correct the long-range energy, and another iterative algorithm is used to obtain desired bulk ionic concentrations.

The systems concerned in the present work contain one species of anion and two species of cations with different diameters but the same valence. The ion density distributions obtained from the DFT are in good agreement with those from the corresponding MC simulations. The results of electrostatic potentials are also presented and the results from the DFT prove to be accurate except that the small divalent cation exists. It should be pointed out that although our DFT performs not very well for small divalent cations, the diameter of realistic divalent cation is usually greater than 0.5 nm.[20] Therefore the accuracy of the DFT prediction of real divalent counterion is as good as the situation of monovalent ions.

We find that the contact value of density profiles and the local mole fraction of cations change greatly as the counterion radius is varied. However, the electrostatic potential has little dependence on the counterion size. The effect of solution composition and ionic diameters on $\psi(R)$ are also investigated in detail. It is found that $\psi(R)$ becomes more positive as the mole fraction of small counterion or the total salt concentration increases. $\psi(R)$ also becomes more positive in the situation when one of counterions becomes smaller, while the size of coion has a contrary effect on $\psi(R)$. The conclusions that can be drawn from a PM study of ion size effects may have severe limitations because of the crudeness of the primitive model itself, where the molecular nature of the solvent is completely neglected. Nevertheless, when we are interested in some integral quantities at low concentrations, the hard-core packing effects between ions can be neglected.

Most of the mobile ions considered in this work may have arbitrary size and valence, and we also illustrate that extending the theory to more realistic models is not very hard. It is prospective to use the present DFT to replace the PB equation in the calculation of thermodynamic properties of aqueous DNA solutions containing concentrated multivalent ions. Whereas there still are some challenges in numerical solution of two- and three-dimensional integral equations presented in Eq. (11).

ACKNOWLEDGMENTS

Project Nos. 20376037 and 20490200 are supported by National Natural Science Foundation of China.

[1] R. V. Gessner, G. J. Quigley, A. H. J. Wang, G. A. van der Maarel, J. H. V. Boom, and A. Rich, Biochemistry **24**, 237 (1985).
[2] T. M. Record, Annu. Rev. Biochem. **50**, 997 (1981).
[3] C. F. Anderson and T. M. Record, Annu. Rev. Phys. Chem. **33**, 191 (1982).
[4] G. R. Pack, L. Wong, and G. Lamm, Biopolymers **49**, 575 (1999).
[5] M. C. Mossing and M. T. Record, Jr., J. Mol. Biol. **186**, 295 (1985).
[6] W. C. Suh, S. Leirmo, and M. T. Record, Jr., Biochemistry **31**, 7815 (1992).
[7] M. W. Capp, D. S. Cayley, W. Zhang, H. J. Guttman, S. E. Melcher, and R. M. Saecker, J. Mol. Biol. **258**, 25 (1996).
[8] J. Shack, R. J. Jenkins, and J. M. Thompsett, J. Biol. Chem. **198**, 85 (1952).
[9] U. P. Strauss, C. Helfgott, and H. Pink, J. Phys. Chem. **71**, 1967 (1967).
[10] H. S. Harned and B. B. Owen, *The Physical Chemistry of Electrolyte Solution* (Reinhold, New York, 1958).
[11] R. L. Kay, in *Water: A Comprehensive Treatise*, edited by F. Franks (Plenum, New York, 1973).
[12] R. Das, T. T. Mills, L. W. Kwok, G. S. Maskel, I. S. Millett, S. Doniach, K. D. Finkelstein, D. Herschlag, and L. Pollack, Phys. Rev. Lett. **90**, 188103 (2003).
[13] S. S. Zakharova, S. U. Eqelhaaf, L. B. Bhuiyan, C. W. Outhwhaite, D. Bratko, and J. R. C. van der Maarel, J. Chem. Phys. **111**, 10706 (1999).
[14] P. Mills, C. F. Anderson, and M. T. Record, Jr., J. Phys. Chem. **89**, 3984 (1985).
[15] H. Ni, C. F. Anderson, and T. M. Record, Jr., J. Phys. Chem. B **103**, 3489 (1999).
[16] J. C. G. Montoro and J. L. F. Abascal, J. Chem. Phys. **103**, 8273 (1995).
[17] M. Le Bret and B. H. Zimm, Biopolymers **23**, 271 (1984).
[18] V. Vlachy and D. J. Haymet, J. Chem. Phys. **84**, 5874 (1986).
[19] N. Korolev, A. P. Lyubartsev, A. Rupprecht, and L. Nordenskiold, J. Phys. Chem. B **103**, 9008 (1999).
[20] N. Korolev, A. P. Lyubartsev, A. Rupprecht, and L. Nordenskiold, Biophys. J. **77**, 2736 (1999).
[21] M. Deserno, F. Jimenez-Angeles, C. Holm, and M. Lozada-Cassou, J. Phys. Chem. B **105**, 10983 (2001).
[22] Z. Tang, L. E. Scriven, and H. T. Davis, J. Phys. Chem. **97**, 494 (1992).
[23] T. Biben, J. P. Hansen, and Y. Rosenfeld, Phys. Rev. E **57**, R3727 (1998).
[24] M. Valisko, D. Henderson, and D. Boda, J. Phys. Chem. B **108**, 16548 (2004).
[25] S. Y. Ponomarev, K. M. Thayer, and D. L. Beveridge, Proc. Natl. Acad. Sci. U.S.A. **101**, 14771 (2004).
[26] K. Anderson, R. Das, H. Y. Park, H. Smith, L. W. Kwok, J. S. Lamb, E. J. Kirkland, D. Herschlag, K. D. Finkelstein, and L. Pollack, Phys. Rev. Lett. **93**, 248103 (2004).
[27] G. S. Manning, Biophys. Chem. **7**, 95 (1977).
[28] G. S. Manning, Q. Rev. Biophys. **11**, 179 (1978).
[29] F. Fogolari, P. Zuccato, G. Esposito, and P. Viglino, Biophys. J. **76**, 1 (1999).
[30] M. Gouy, J. Phys. Theor. Appl. **9**, 457 (1910).
[31] D. L. Chapman, Philos. Mag. **25**, 475 (1913).
[32] B. Jayaram and D. L. Beveridge, Annu. Rev. Phys. Chem. **25**, 367 (1996).
[33] M. Fixman, J. Chem. Phys. **70**, 4995 (1979).
[34] S. L. Carnie and G. M. Torrie, Adv. Chem. Phys. **56**, 141 (1984).
[35] L. Degreve and M. Lozada-Cassou, Mol. Phys. **86**, 759 (1995).
[36] C. W. Outhwhaite and L. B. Bhuiyan, Mol. Phys. **74**, 367 (1991).
[37] L. B. Bhuiyan and C. W. Outhwhaite, J. Chem. Phys. **116**, 2650 (2002).
[38] T. Das, D. Bratko, L. B. Bhuiyan, and C. W. Outhwhaite, J. Chem. Phys. **107**, 9197 (1997).
[39] E. Gonzalez-Tovar and M. Lozada-Cassou, J. Phys. Chem. **93**, 3761 (1989).
[40] Y.-X. Yu, J. Wu, and G.-H. Gao, J. Chem. Phys. **120**, 7223 (2004).
[41] M. Lozada-Cassou, R. Saavedra-Barrera, and D. Henderson, J. Chem. Phys. **77**, 5150 (1982).
[42] G. N. Patey, J. Chem. Phys. **72**, 5763 (1980).
[43] L. Yeomans, S. E. Feller, E. Sanchez, and M. Lozada-Cassou, J. Chem. Phys. **98**, 1436 (1993).
[44] G. I. Guerrero-Garcia, E. Gonzalez-Tovar, M. Lozada-Cassou, and F. D. Guegara-Rodriguez, J. Chem. Phys. **123**, 034703 (2005).
[45] M. Lozada-Cassou, R. Evans *et al.*, *Fundamentals of Inhomogeneous Fluids* (Marcel Dekker, New York, 1992).
[46] Y.-X. Yu and J. Wu, J. Chem. Phys. **117**, 10156 (2002).
[47] Y. Rosenfeld, Phys. Rev. Lett. **63**, 980 (1989).
[48] Y. Rosenfeld, J. Chem. Phys. **93**, 4305 (1990).
[49] Y. Rosenfeld, J. Chem. Phys. **98**, 8126 (1993).
[50] C. N. Patra and A. Yethiraj, J. Phys. Chem. B **103**, 6080 (1999).
[51] D. Gillespie, W. Nonner, and R. S. Eisenberg, J. Phys.: Condens. Matter **14**, 12129 (2002).
[52] D. Gillespie, W. Nonner, and R. S. Eisenberg, Phys. Rev. E **68**, 031503 (2002).
[53] O. Pizio, A. Patrykiejew, and S. Sokolowski, J. Chem. Phys. **121**, 11957 (2004).
[54] J. Reszko-Zygmunt, S. Sokolowski, D. Henderson, and D. Boda, J. Chem. Phys. **122**, 084504 (2005).
[55] C. N. Patra and S. K. Ghosh, J. Chem. Phys. **117**, 8938 (2002).
[56] D. Boda, W. R. Fawcett, D. Henderson, and S. Sokolowski, J. Chem. Phys. **116**, 7170 (2002).
[57] C. N. Patra and A. Yethiraj, Biophys. J. **78**, 699 (2000).
[58] K. Wang, Y.-X. Yu, and G.-H. Gao, Phys. Rev. E **70**, 011912 (2004).

[59] T. Nishio and A. Minakata, J. Chem. Phys. **113**, 10784 (2000).
[60] K. Hiroke, Mol. Phys. **33**, 1195 (1977).
[61] J. Forsman, J. Phys. Chem. B **108**, 9236 (2004).
[62] R. Penfold, S. Nordholm, B. Jonsson, and C. E. Woodward, J. Chem. Phys. **92**, 1915 (1990).
[63] L. Guldbrand, B. Jonsson, H. Wennerstron, and P. Linse, J. Chem. Phys. **80**, 2221 (1984).
[64] M. P. Allen and D. J. Tildesley, *Computer Simulation of Liquids* (Oxford University Press, New York, 1987).
[65] C. Murthy, R. J. Bacquet, and P. J. Rossky, J. Phys. Chem. **89**, 701 (1985).
[66] D. Boda, K.-Y. Chan, and D. Henderson, J. Chem. Phys. **109**, 7362 (1998).
[67] D. Boda, D. D. Busath, D. Henderson, and S. Sokolowski, J. Phys. Chem. B **104**, 8903 (2000).
[68] D. Boda, D. Henderson, and D. D. Busath, J. Phys. Chem. B **105**, 11575 (2001).
[69] Y. W. Tang and K.-Y. Chan, Mol. Simul. **30**, 63 (2004).